MATHEWS

Case Reports

Mathews Journal of Case Reports

Adaptive Cytokine- and Exosome-Based Therapy for Coexisting Vascular Dementia and Prostate Cancer: A Case Report

Takuji Shirasawa[1,2]*, Luis Carlos Aguilar Cobos[3]

[1]*Ochanomizu Health and Longevity Clinic, Tokyo 101-0062, Japan*

[2]*Shirasawa Anti-Aging Medical Institute, Tokyo 101-0062, Japan*

[3]*Livant Neurorecovery Center, Guadalajara, Mexico*

ABSTRACT

Background: The coexistence of vascular dementia and prostate cancer poses therapeutic challenges because standard oncological interventions may affect cognition, whereas neuroregenerative growth factors may influence tumor biology. This report describes longitudinal cytokine- and exosome-based treatment in a patient with both conditions.

Case Presentation: A 78-year-old man presented with memory impairment and vascular risk factors, including hypertension, dyslipidemia, and type 2 diabetes mellitus. Baseline evaluation showed an MMSE score of 27/30, impaired verbal memory, slow-wave EEG activity, abnormal P300 responses, cortical and hippocampal atrophy, subcortical vascular lesions, carotid intraluminal atherosclerotic findings, and elevated PSA. He received sublingual cytokine- and exosome-based formulations, with serial cognitive testing, EEG, MRI, carotid virtual endoscopy, PSA monitoring, prostate biopsy, and bone scintigraphy.

Results: During neuroregenerative therapy, global cognitive function remained broadly stable for several years, although verbal memory later declined. Follow-up EEG demonstrated reduced slow-wave activity and interval changes in P300 responses, while MRI showed persistent cortical atrophy, resolution of some subcortical vascular abnormalities, hippocampal morphological changes, and regression of carotid intraluminal lesions. Prostate biopsy confirmed adenocarcinoma in 5 of 16 specimens, with an overall Gleason score of 4+3=7. After PSA elevation, IGF-containing formulations were replaced with an anti-oncogenic cytokine and exosome cocktail. PSA levels subsequently remained relatively stable, and MRI and bone scintigraphy showed no evidence of local invasion or bone metastasis.

Conclusion: Longitudinal observations suggest that cytokine- and exosome-based regimens may be adaptable to the competing priorities of vascular dementia and prostate cancer by removing growth-promoting

Vol No: 11, Issue: 04

Received Date: September 09, 2026

Published Date: September 24, 2026

***Corresponding Author**

Takuji Shirasawa,

Ochanomizu Health and Longevity Clinic, Tokyo 101-0062, Japan, and Shirasawa Anti-Aging Medical Institute, Tokyo 101-0062, Japan, E-mail: takujishirasawa@icloud.com

Citation: Shirasawa T, Cobos LCA. (2026). Adaptive Cytokine- and Exosome-Based Therapy for Coexisting Vascular Dementia and Prostate Cancer: A Case Report. Mathews J Case Rep. 11(4):233.

components and emphasizing anti-oncogenic signaling pathways. However, this single case cannot establish efficacy or causality, and controlled studies are required to confirm these findings.

Keywords: Vascular Dementia, Prostate Cancer, Anti-Oncogenic Cytokines, Exosomes

INTRODUCTION

The coexistence of vascular dementia and prostate cancer represents an increasingly important clinical dilemma in aging societies [1]. Vascular dementia arises from cumulative cerebrovascular injury and is frequently accompanied by hypertension, diabetes mellitus, dyslipidemia, and systemic atherosclerosis [2]. Although vascular risk modification remains the cornerstone of management, many patients continue to experience progressive cognitive decline, highlighting the need for complementary strategies that target neurovascular repair, inflammation, and neuronal network dysfunction [3].

Cytokine- and exosome-based interventions have emerged as biologically plausible tools for modulating tissue repair, immune signaling, vascular remodeling, and intercellular communication [4-6]. Exosomes deliver microRNAs, proteins, and lipids that may influence regenerative and protective pathways, while selected cytokines may support neuroimmune and vascular homeostasis [7]. However, this therapeutic concept becomes more complex when malignancy is present [8]. Growth factor–containing formulations, including those with IGF-related activity, may theoretically enhance tumor-cell proliferation and therefore require careful reassessment in patients with active or suspected cancer [9].

Prostate cancer is highly prevalent among elderly men, many of whom also have cognitive and cardiovascular comorbidities [10]. Conventional treatments such as androgen deprivation therapy and radiotherapy can be effective for cancer control, but they may be associated with systemic adverse effects and cognitive concerns in vulnerable patients [1,11]. Thus, the simultaneous management of prostate cancer and dementia requires a therapeutic framework that avoids accelerating either neurological decline or tumor progression [1,11].

Here, we report the longitudinal course of a 78-year-old man with vascular dementia complicated by biopsy-confirmed prostate cancer. The case is notable because the cytokine- and exosome-based regimen was adapted from a neuroregenerative formulation to an anti-oncogenic cocktail after PSA elevation and pathological confirmation of malignancy. We present serial cognitive, electrophysiological, vascular, prostate imaging, histopathological, and PSA findings, and discuss this case as a model for the precision modulation of regenerative therapy when neurodegenerative and oncological priorities compete within the same patient.

To our knowledge, this case illustrates a clinically relevant example of adaptive cytokine- and exosome-based regimen modification in a patient with concurrent vascular dementia and biopsy-confirmed prostate cancer, highlighting the need to balance neuroregenerative goals with oncological safety.

METHODS

The cytokine and exosome cocktail used in this case study was designed and developed by Luis Carlos Aguilar Cobos at the Livant Neurorecovery Center, Mexico, as previously described [5,6,12-14]. Eleven cytokine- and exosome-based formulations were administered as shown in Figure 1. The formulations included components selected for their potential relevance to GABAergic (Gabatrof) and glutamatergic (Epatrof) neurogenesis. OST formulations contained progranulin, a factor implicated in neurogenic processes in the frontal and temporal cortices. CAL contained VEGF for vascular regeneration, Renotrof contained soluble α-klotho for endothelial protection, LEU contained IL-12 for immune enhancement, and ADPK contained adiponectin for insulin sensitivity and endothelial protection. Neurogen Cortex contained miRNAs selected for potential anti-oncogenic activity, and Meta Di Reg contained FGF21 for metabolic modulation. Treatment was administered sublingually three times daily.

CASE DESCRIPTION

Initial Assessment

A 78-year-old man from Yamanashi presented to the Ochanomizu Health and Longevity Clinic on June 10, 2019, with subjective memory complaints. His medical history included a herniated disk at 68 years of age and hypertension, dyslipidemia, and type 2 diabetes mellitus diagnosed at 74 years of age. Neurological examination on the same day revealed moderate memory impairment. The Mini-Mental State Examination score was 27/30, and the Cognitrax total score was 80.2. Cognitrax domain scores were 17 for verbal

memory, 105 for reasoning, 88 for executive function, 87 for cognitive flexibility, 73 for reaction time, 111 for motor speed, 97 for attention, and 85 for working memory (Figure 1).

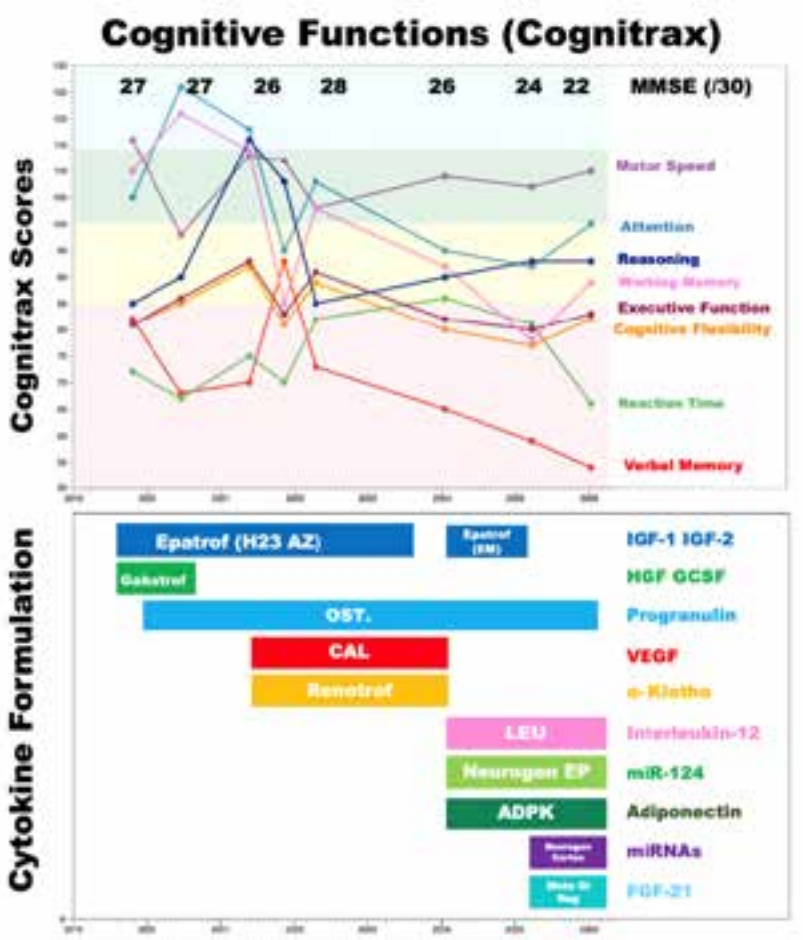

Figure 1: Cognitive function was assessed using Cognitrax and the Mini-Mental State Examination (MMSE) at seven time points: June 10, 2019; October 17, 2019; June 18, 2020; November 8, 2021; April 14, 2022; March 24, 2025; and January 21, 2026. MMSE scores are shown in the upper part of the graph. Cognitrax scores are plotted chronologically for cognitive flexibility (orange), executive function (brown), working memory (magenta), attention (light blue), reasoning (dark blue), reaction time (green), motor speed (plum), and verbal memory (red). Green indicates the mean ±1 standard deviation (SD), yellow indicates −1 to −2 SD below the mean, red indicates more than −2 SD below the mean, light blue indicates +1 to +2 SD above the mean, and blue indicates more than +2 SD above the mean. A cognitive score of 100 represents the average score for an age-matched Japanese population. Administered cytokines and exosomes are shown below the graph.

At presentation, the patient was receiving esomeprazole 20 mg once daily each morning, amlodipine 2.5 mg once daily each morning, and omega-3-acid ethyl esters 2 g twice daily in the morning and evening from a local hospital.

Baseline laboratory evaluation, including complete blood count and blood chemistry testing, showed preserved hepatic, renal, and hematopoietic function, with no evidence of nutritional deficiency. Serum lipid testing showed total cholesterol of 163 mg/dL, triglycerides of 100 mg/dL, high-density lipoprotein (HDL) cholesterol of 53 mg/dL, and low-density lipoprotein (LDL) cholesterol of 94 mg/dL. Fasting blood glucose was 116 mg/dL, hemoglobin A1c was 5.3%, serum B-type natriuretic peptide (BNP) was 18.8 pg/mL, and prostate-specific antigen (PSA) was 5.42 ng/mL. Genetic analysis identified an APOE ε3/ε3 genotype.

Electroencephalography performed on June 10, 2019, showed resting slow-wave activity in the frontal, occipital, and parietal leads (data not shown). Analysis of P300 EEG data using Neuroscan software demonstrated hypoactive responses with asymmetric peaks in the frontal and frontopolar leads following target stimulation with a low-pitched sound (Figure 2A, red line). Higher-magnification

assessment of P300 responses in the frontopolar leads showed asymmetric low-voltage responses (Figure 2B). Coherence analysis of the P300 revealed elevated frontal connectivity with limited variability in the frontopolar and frontal leads, findings that may be consistent with reduced inhibitory network function in these regions (Figure 2C, left panel). During cognitive tasks, including the attention test, emotional processing test, visuospatial memory test (Figure 2D, red line), and mental flexibility test using the Wisconsin Card Sorting Test, EEG response amplitudes were reduced.

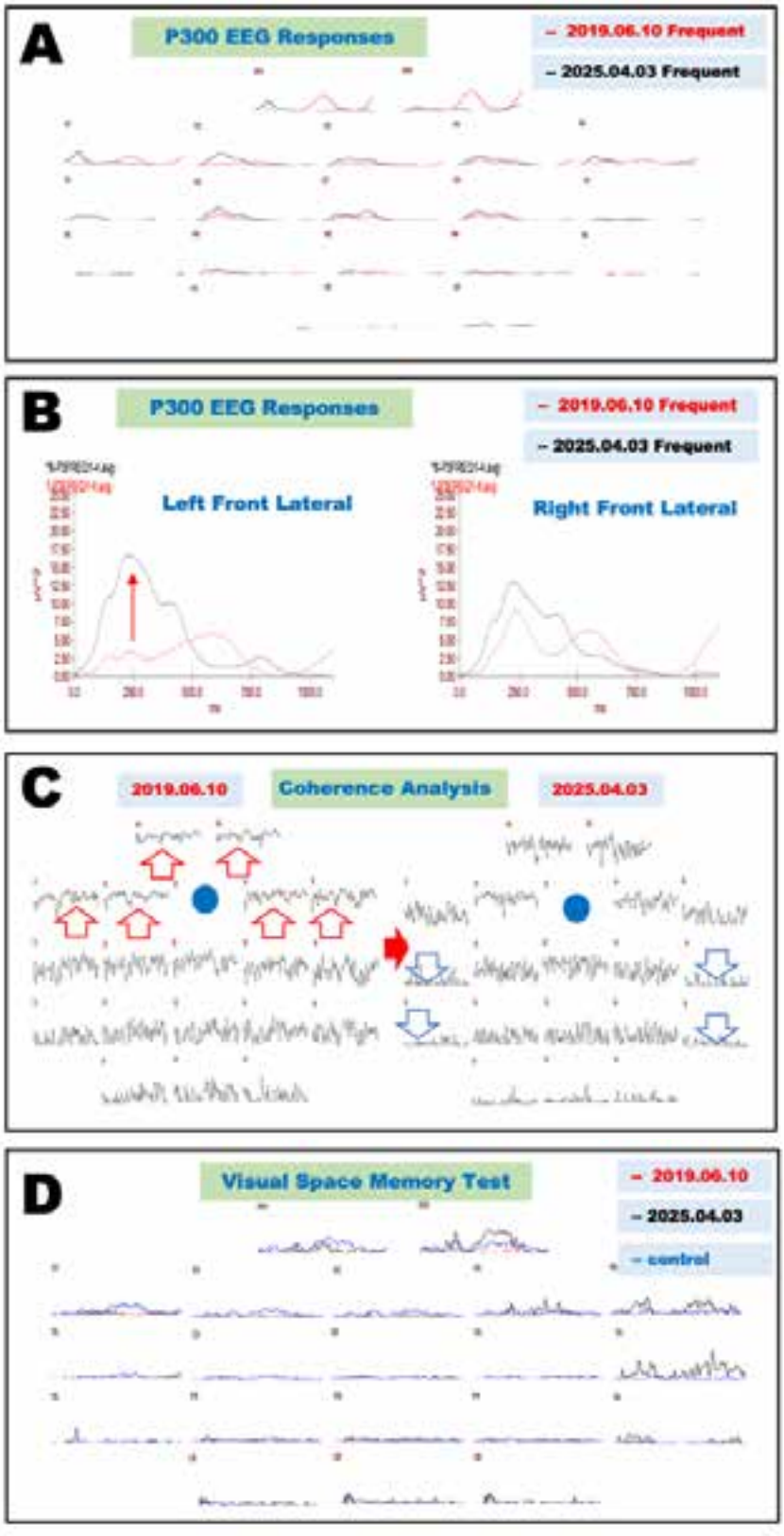

Figure 2:

A: Electrophysiological evaluation of P300 electroencephalogram (EEG) responses during cytokine-based treatment. Prior to treatment, on June 10, 2019, the P300 EEG responses to a frequent stimulus (low-pitched sound) are shown as red lines. Following treatment, on April 3, 2025, the EEG responses are illustrated as black lines.

B: A magnified view of the recordings from the frontopolar electrodes is presented. The P300 responses recorded on April 3, 2025 (black lines) appeared to be increased compared with those recorded on June 10, 2019 (red lines; left, left frontopolar leads; right, right frontopolar leads).

C: Coherence analysis of P300 responses at baseline and follow-up during cytokine-based therapy. Analysis of neural network connectivity in the frontopolar electrodes (FP1 and FP2, indicated by red arrows) showed enhanced connectivity by April 3, 2025, compared with June 10, 2019. The amplitude was slightly depressed in both temporal leads (T3, T4, T5, and T6, indicated by blue arrows).

D: Electroencephalographic (EEG) recordings during the visuospatial memory test at baseline and follow-up during cytokine therapy. The flattened responses observed on June 10, 2019 (red) were enhanced on April 3, 2025 (black dashed line). Blue indicates the control group.

Analysis of MRI data acquired on June 10, 2019, revealed mild cortical atrophy in the parietal, temporal, and frontal lobes, with widening of the Sylvian fissure (Figure 3A). A sagittal section of the left hemisphere showed scattered subcortical vascular lesions (Figure 3B, red arrow, red and yellow circles). Hippocampal morphology was assessed using MRI-based virtual endoscopic images acquired on June 10, 2019. These images showed apparent atrophy of the head and neck portions of both hippocampi (Figures 4A and 4B). Mild bilateral atrophy of the entorhinal cortex (EC) was also observed in the temporal cortices (Figures 4A and 4B). As illustrated in Figure 5, virtual endoscopic images demonstrated intraluminal material adherent to the endothelial surface within the bilateral internal carotid arteries (Figures 5A, 5C, and 5E). Based on their morphology and vascular location, these lesions were considered compatible with atherosclerosis associated with diabetes and dyslipidemia.

Taken together, the clinical, imaging, laboratory, and electrophysiological findings were consistent with vascular brain pathology associated with impaired memory function. Based on the clinical history, the underlying vascular pathology may have been related, at least in part, to diabetes mellitus and dyslipidemia.

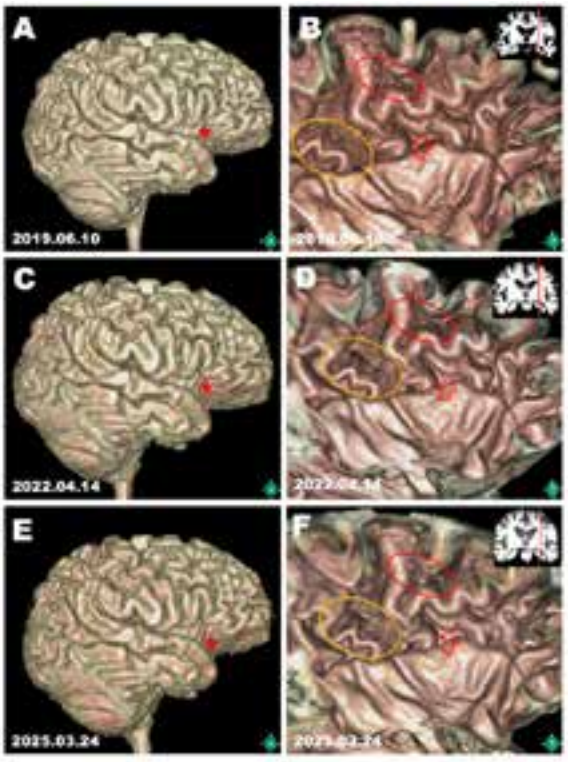

Figure 3: MRI scans were acquired on June 10, 2019; April 14, 2022; and March 24, 2025, before and during follow-up after cytokine-based therapy. Panels A, C, and E show three-dimensional reconstructions of the cerebral cortex, presented as lateral views of the right hemisphere, generated in silico from T1-weighted MRI data with 1-mm sagittal slices using Expert INTAGER software. Panels B, D, and F show cut-surface images of the left prefrontal region corresponding to the red lines shown in the upper-right insets. Red arrows and red and yellow circles indicate subcortical vascular lesions, and red asterisks indicate the Sylvian fissures.

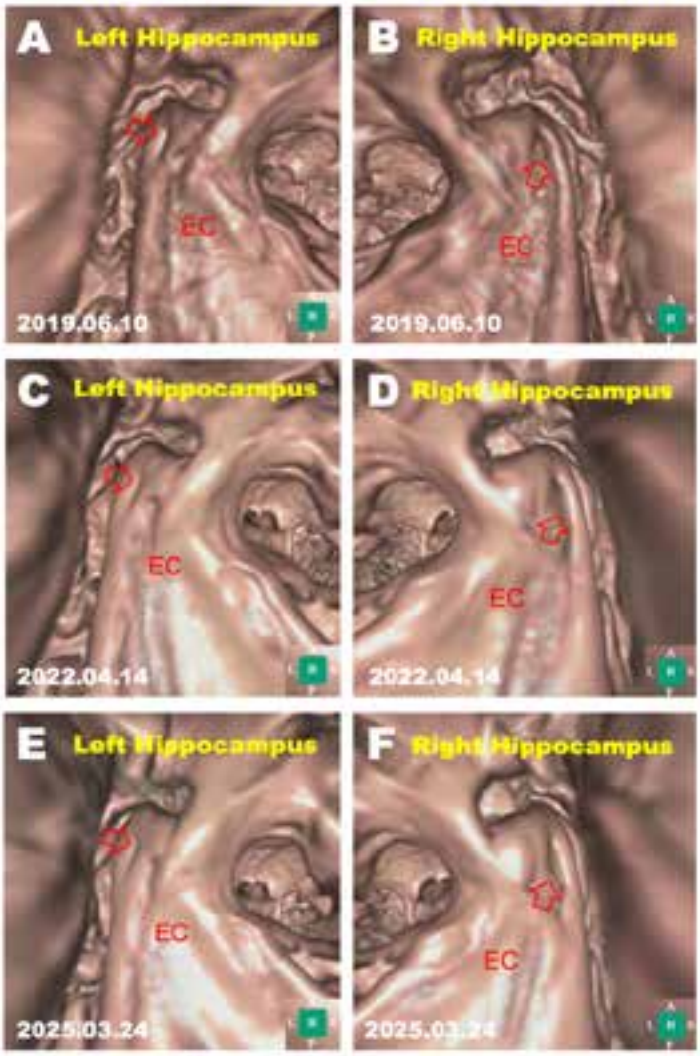

Figure 4: Morphological evaluation of the hippocampus before and during follow-up after cytokine-based treatment. Panels A and B show in silico endoscopic images of the left (A) and right (B) hippocampus obtained on June 10, 2019, demonstrating atrophy of the hippocampal neck. Panels C–F show corresponding follow-up in silico endoscopic images of the left (C, E) and right (D, F) hippocampus obtained on April 14, 2022, and March 24, 2025, respectively, demonstrating interval morphological changes in the hippocampal neck. Arrows indicate regions of structural change. EC, entorhinal cortex.

Cytokine-Based Regenerative Treatment for Vascular Dementia

The cytokine-based therapy protocol comprised Epatrof (H23 AZ), threefold concentration, 2.0 mL; Gabatrof (EPI), threefold concentration, 2.0 mL; OST, threefold concentration, 2.0 mL; CAL, threefold concentration, 2.0 mL; and Renotrof (23), threefold concentration, 1.0 mL. Each formulation was administered three times daily from June 10, 2019, to January 15, 2024. The treatment period is shown in the lower panel of Figure 1. The clinical protocol and formulations were developed at the Livant Neurorecovery Center in Mexico, as previously described [6,13].

As shown in Figure 1, serial cognitive assessments were performed during long-term cytokine-based therapy. During this period, the overall Cognitrax profile showed no marked deterioration, with a follow-up score of 87.4 compared

with 91.5 at baseline. Motor speed improved across serial assessments, whereas other domains—including cognitive flexibility, attention, working memory, and reasoning—remained broadly stable. In contrast, verbal memory began to decline in 2022 and continued to deteriorate thereafter, as shown in Figure 1. Although the MMSE score increased to 28/30 on April 14, 2022, it subsequently decreased to 22/30 on January 21, 2026. Both the MMSE score and the Cognitrax verbal memory score deteriorated after the cytokine strategy was changed from a neuroregenerative approach to a neuroprotective and anti-oncogenic cocktail, as shown in Figures 1 and 7.

A follow-up electroencephalogram (EEG) obtained on April 3, 2025, showed reduced slow-wave activity compared to the baseline study (data not shown). P300 EEG responses also changed over time; responses in the frontopolar leads were enhanced (Figure 2B, red arrow), whereas low-voltage P300 responses were observed in the frontal, central, right parietal, and right occipital leads (Figure 2A, red lines). These findings may be compatible with the partial restoration of excitatory neuronal network activity; however, the underlying mechanism cannot be determined from a single case.

Coherence analysis of P300 signals recorded on April 3, 2025, showed interval changes in frontopolar and frontal network connectivity compared with baseline (Figure 2C). Although these findings may be consistent with changes in inhibitory network function, any inference regarding GABAergic neurogenesis or synaptic restoration remains speculative in a single-case report. In the visuospatial memory test, the reduced response observed on June 10, 2019 (Figure 2D, red line) was enhanced on April 3, 2025 (Figure 2D, black line), although the response remained greater than the control response. These findings are compatible with interval changes in visuospatial electrophysiological measures during follow-up, but they do not permit firm conclusions regarding treatment effect.

MRI performed on April 14, 2022, and March 24, 2025, showed a similar degree of atrophy in the frontal, temporal, and parietal cortices compared with the baseline study (Figures 3C and 3E). Sagittal cut sections of the left hemisphere showed resolution of the vascular abnormalities observed in the initial study (Figures 3D and 3F). In contrast, in silico endoscopic assessment of the hippocampus demonstrated interval morphological changes in the bilateral hippocampi compared with baseline images (Figures 4D and 4F). These findings may be compatible with localized structural remodeling; however, they do not establish hippocampal regeneration, and any relationship to cognitive performance should be interpreted cautiously.

For the carotid intraluminal findings, the cytokine-based vascular regenerative treatment protocol was administered from May 20, 2021, to March 24, 2025 (Figure 1). Virtual endoscopy demonstrated that the atherosclerotic lesions observed on June 10, 2019, decreased in size by March 24, 2025 (Figures 5D and 5F). These imaging findings are compatible with interval regression of the lesions; however, their precise composition cannot be determined from imaging alone.

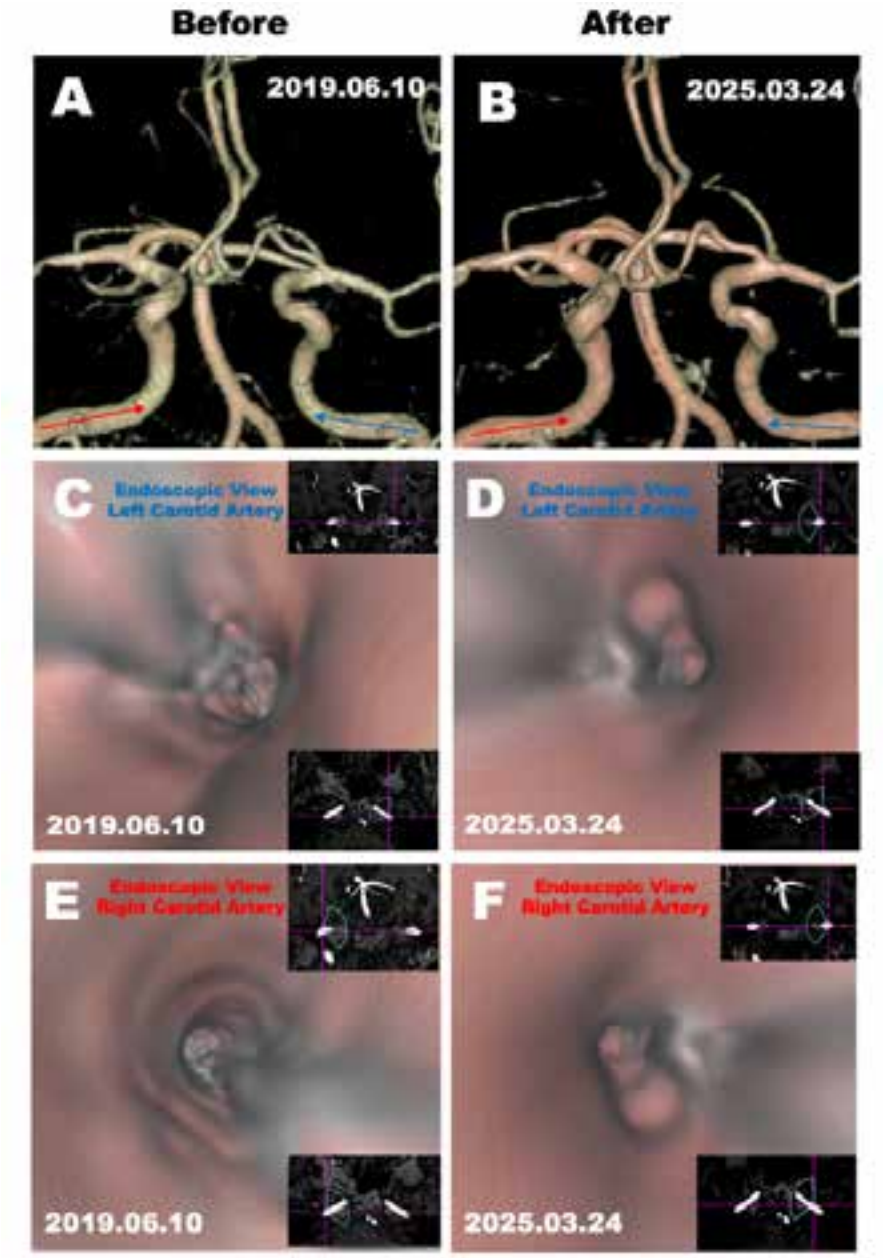

Figure 5: Three-dimensional (3D) computer-generated images show carotid atherosclerotic pathologies in the right and left carotid arteries (A, C, E) obtained on June 10, 2019, before cytokine-based treatment. The corresponding follow-up images are shown in panels B, D, and F. The upper and lower right insets show the position and viewing window of the in silico camera within the carotid artery (C, D, E, F). The red and blue arrows in the 3D MRA view (A and B) indicate the axis of the endoscopic views shown in C, D, E, and F.

Prostate cancer complicated by vascular dementia

As the patient had an elevated PSA level from the initial visit, cytokine-based neuroregenerative therapy was administered with careful monitoring. In particular, because the treatment cytokine formulation contained IGF-1 and IGF-2, which may promote prostate cancer cell proliferation, a prostate biopsy was performed in 2021 at the Department of Urology, Juntendo University, after the PSA level exceeded 9.0 ng/mL.

As shown in Table 1, a total of 16 prostate biopsy specimens were obtained from the right and left lobes. Histopathological examination identified lesions diagnostic of prostate cancer in samples #1, #2, #9, #12, and #13. According to the pathological assessment, samples #1, #2, and #13 were assigned a Gleason score of 3+3, sample #12 was assigned a Gleason score of 4+3, and sample #9 was assigned a Gleason score of 4+4. Based on these findings, the patient was diagnosed with prostate cancer, with an overall Gleason score of 4+3=7.

Table 1. Gleason score of prostate biopsy specimens

Sample	Lobe	Location	Size (mm)	Pathology (GS)
#1	Right lobe	Lateral peripheral margin	5.0 × 11.0	3+3
#2	Right lobe	Lateral	0.5 x 9.0	3+3
#3	Right lobe	Medial	none	-
#4	Right lobe	Medial	none	-
#5	Right lobe	Lateral		Atypical gland
#6	Right lobe	Medial	none	-
#7	Left lobe	Lateral peripheral margin	none	-
#8	Left lobe	Lateral	none	-
#9	Left lobe	Medial	2.0 × 14.0	4+4
#10	Left lobe	Lateral	none	-
#11	Left lobe	Lateral	none	-
#12	Left lobe	Medial	7.0 x 13.0	4+3
#13	Right lobe	Anterior	1.0 x 10.0	3+3
#14	Right lobe	Anterior	none	-
#15	Left lobe	Anterior	none	-
#16	Left lobe	Anterior	none	-

* Adenocarcinoma was identified in five of 16 biopsy sites, with an overall Gleason score of 4+3=7.

** Histology of sample #9 is shown in Figure 6A, 6B, 6C, and 6D.

*** Histology of sample #13 is shown in Figure 6E and 6F.

Clinical diagnosis was performed by urologists Haruna Kono and Shigeo Horie at Juntendo University.

Pathological diagnosis was performed by Yoshiki Kuwatsuru and Nobuo Tomizawa of Juntendo University.

Figure 6 shows representative microscopic images of prostate biopsy specimens. Panels 6A and 6C show histopathological images of prostate cancer in sample #9, and panels 6B and 6D show higher-magnification views of panels 6A and 6C, respectively. Irregular glandular architecture and nuclear atypia were consistent with adenocarcinoma. Panel 6E shows a histopathological image of biopsy sample #13, and panel 6F shows a higher-magnification view of panel 6E. This specimen also showed adenocarcinoma with disrupted glandular architecture. In both samples, disorganized epithelial alignment and prominent nuclear atypia were observed. In sample #9, clusters of cancer cells were present within the glandular lumen, a finding that may suggest intraductal spread or a more aggressive histopathological pattern.

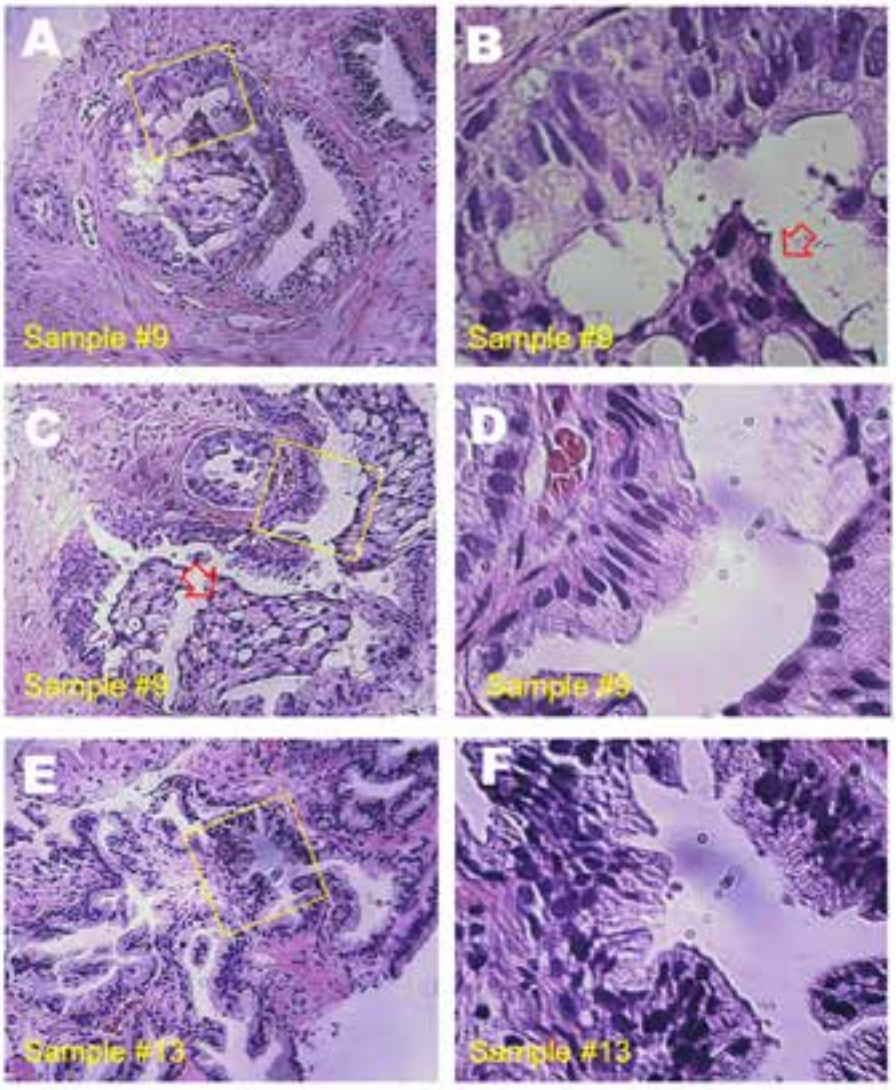

Figure 6: Histopathological images of prostate biopsy specimens. Panels A and C show malignant histopathological findings in sample #9, and panels B and D show higher-magnification views of the corresponding boxed areas. Panel E shows malignant histopathological findings in sample #13, and panel F shows a higher-magnification view of the area indicated by the yellow box in panel E. Red arrows indicate intraductal carcinoma of the prostate (IDCP).

Bone scintigraphy was performed at the Juntendo University School of Medicine in January 2025. No evidence of bone metastasis from prostate cancer was detected. The isotope uptake seen on the anterior radionuclide image in Figure 7 was localized to the sternum and was therefore considered unlikely to represent metastatic disease; instead, it was interpreted as probable isotope accumulation related to sternal trauma.

Additional MRI-based evaluation of the prostate was performed. Compared with images acquired on March 15, 2021, images acquired on August 25, 2026, showed no prostate enlargement, extracapsular extension, or invasion into adjacent organs. No irregularity of the internal architecture of either prostate lobe was observed. Figures 8C and 8D show three-dimensional MRI reconstructions of the prostate: panel 8C presents an anterior view of the prostate, bladder, and testes, whereas panel 8D presents a right lateral view. Panel 8E shows a cutting-surface reconstruction visualizing the interface between the prostate and bladder, with no evidence of local invasion into the bladder. Panel 8F shows a virtual MRI image of the bladder mucosa viewed from the upper-left oblique direction, also supporting the absence of bladder mucosal invasion.

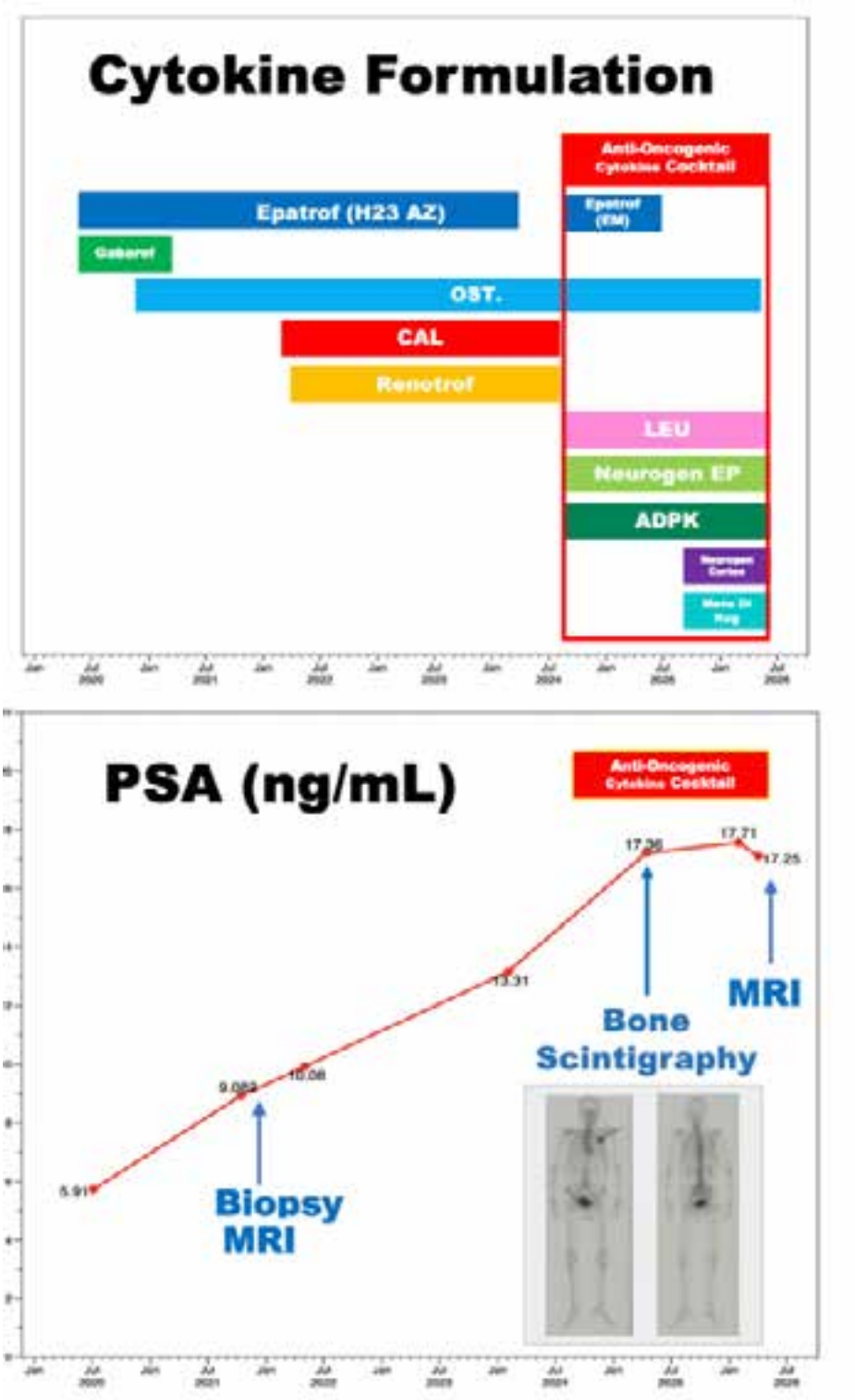

Figure 7: Cytokine-based anti-oncogenic treatment protocol for prostate cancer and longitudinal changes in PSA levels. The upper panel shows the formulation of the cytokine cocktail. The lower panel shows longitudinal changes in PSA levels and the timelines of prostate biopsy, bone scintigraphy, and MRI examinations.

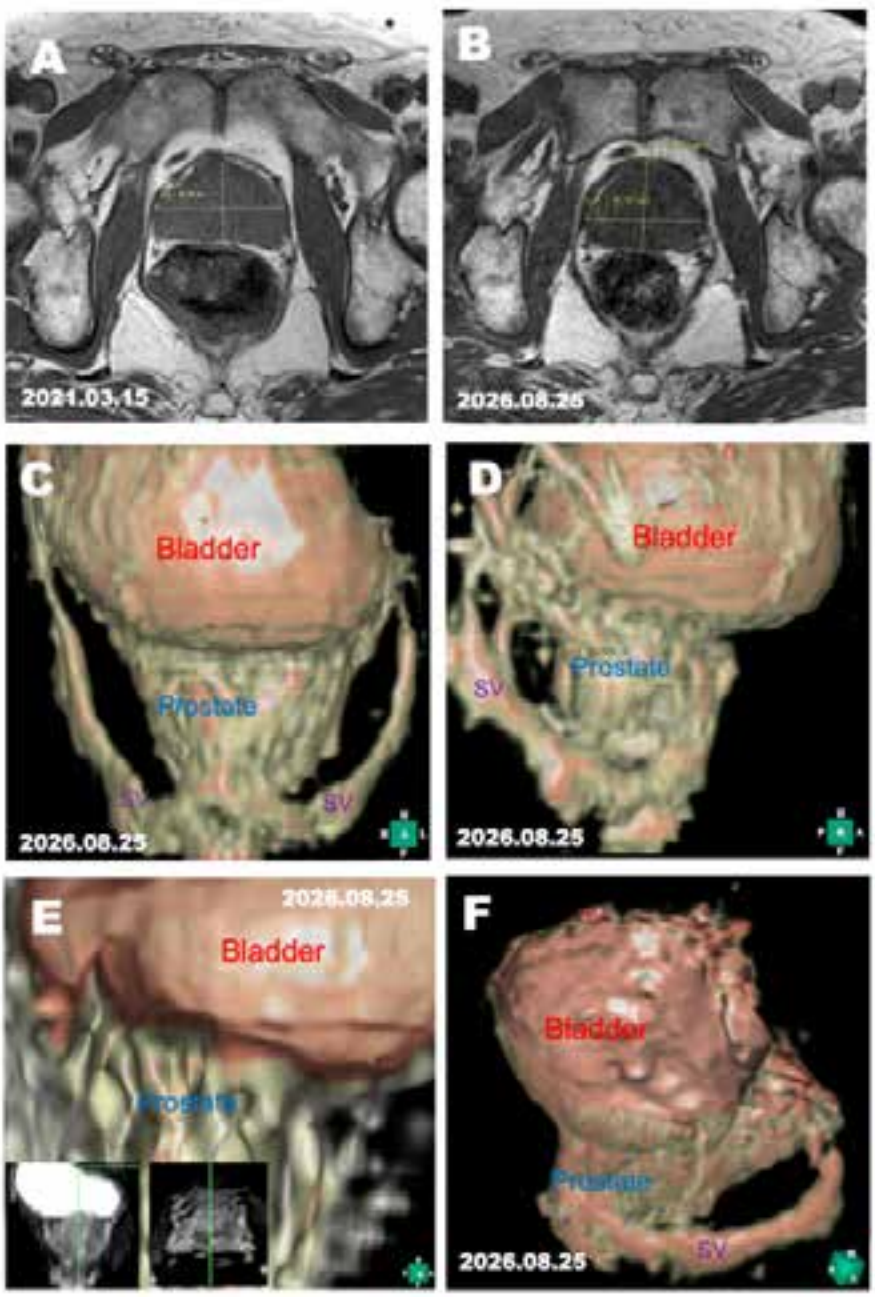

Figure 8: MRI images before and after cytokine-based anti-oncogenic treatment. Panels A and B show prostate MRI images obtained on March 15, 2021, and August 25, 2026, respectively. Panels C–F show 3D MRI images obtained on August 25, 2026: an anterior view (C), a right lateral view (D), a central cutting-section image (E), and a 3D image showing the bladder mucosa viewed from the upper-left oblique direction (F).

Anti-Oncogenic Cytokine-Based Treatment for Prostate Cancer

After switching to this regimen, serial PSA monitoring showed relative stabilization of PSA levels: 17.38 ng/mL in January 2025, 17.71 ng/mL in January 2026, and 17.25 ng/mL in March 2026. In addition, MRI performed on August 25, 2026, showed no evidence of prostate cancer progression, and bone scintigraphy showed no evidence of bone metastasis. Although cognitive function was monitored during this period, subsequent decline in MMSE and verbal memory indicates that neurological stability was incomplete. This cytokine strategy was therefore intended to balance cognitive preservation with limitation of prostate cancer progression, but its clinical effect cannot be established from this single case.

DISCUSSION

This case illustrates the therapeutic complexity of managing vascular dementia in an elderly patient who subsequently developed biopsy-confirmed prostate cancer. The main clinical challenge was that neuroregenerative therapy and oncological safety required partially opposing biological considerations. The initial cytokine- and exosome-based regimen was selected to support neurovascular repair, neuronal network activity, and vascular remodeling. During follow-up, global cognitive performance remained relatively stable for several years, P300 EEG responses showed interval changes, subcortical vascular lesions appeared reduced, and carotid intraluminal abnormalities regressed on virtual endoscopic imaging. These observations are compatible with possible changes in neurovascular and electrophysiological markers during treatment; however, they should be interpreted cautiously because spontaneous fluctuation, background medical management, measurement variability, and imaging variability cannot be excluded.

The diagnosis of prostate cancer required reassessment of the regenerative strategy. In prostate cancer, growth factor signaling, including IGF-1 and IGF-2 pathways, may contribute to tumor proliferation and disease progression [8,9,15]. Therefore, the continued use of IGF-containing formulations was considered biologically inappropriate after PSA elevation and pathological confirmation of adenocarcinoma. As shown in Figure 7, the therapeutic strategy was consequently shifted from a neuroregenerative cocktail to an anti-oncogenic cytokine and exosome regimen. Following this change, PSA levels remained relatively stable, and MRI and bone scintigraphy showed no evidence of local invasion or bone metastasis. Although these findings do not prove antitumor efficacy, they support the concept that cytokine-based formulations can be adaptively modified according to cancer risk.

As illustrated in Figures 9 and 10, this case required a molecular system-normalization framework capable of reconciling tumor suppression with vascular homeostasis. The vascular-stability axis was designed to preserve cerebral microcirculation and prevent vascular cognitive decline using adiponectin, α-klotho, and FGF21 (Figure 9 and 10). Adiponectin activates AMPK and suppresses mTOR signaling [16], α-klotho inhibits IGF-1, Wnt, and TGF-β–mediated tumor-growth networks [17], and FGF21 improves lipid metabolism while enhancing adiponectin expression [18]. Given its ability to suppress anabolism and induce AMPK signaling, adiponectin was prioritized as Tier 1, followed by soluble α-klotho and FGF21 as Tiers 2 and 3, respectively. In parallel, the tumor-suppression axis was constructed through prioritized miRNA-mediated silencing, including miR-34a/let-7 for stemness and proliferation, miR-145 for androgen signaling, and miR-205 for invasion and epithelial–mesenchymal transition [19-21]. These miRNAs target key oncogenic networks involving CD44, MYC, Cyclin D1, RAS, HMGA2, AR, KRAS, SRC, FAK, and ZEB/EMT [19,22-24]. Additional epigenetic normalization was incorporated through miR-101-mediated regulation of EZH2 and miR-29-mediated modulation of DNMT3A/3B [25,26], thereby targeting tumor growth and fibrosis. miR-124, contained in Neurogen EP, was included because of its dual neuroprotective and anti-oncogenic potential [27]. It may contribute to stabilization of the neuronal phenotype and neuroprotection through regulation of microglial activation, while also suppressing prostate cancer–related pathways through inhibition of AR, AR-V7, and EZH2 [28]. Finally, IL-12 was added as an immune-activation axis. As a major component of Leu, IL-12 binds IL-12Rβ1/β2 on immune cells, activates JAK2/TYK2 signaling, phosphorylates STAT4, and induces IFN-γ production [29,30]. Through this pathway, IL-12 promotes NK-cell, CD8+ T-cell, and Th1-cell activation and enhances secretion of tumor-cytotoxic mediators, including perforin and granzyme [31].

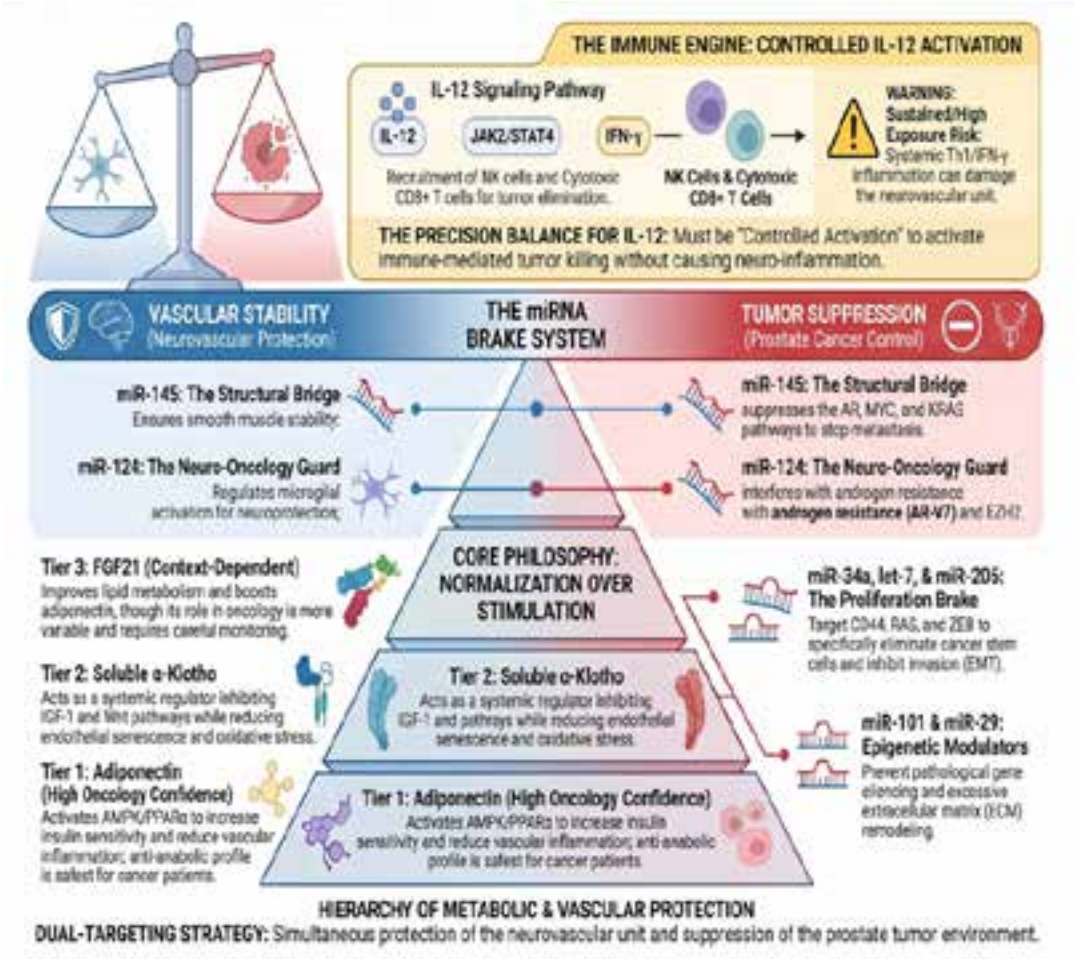

Figure 9: A molecular normalization strategy for coexisting vascular dementia and prostate cancer, illustrating the coordinated use of vascular-stability, tumor-suppression, epigenetic-normalization, neuroprotective, and immune-activation axes.

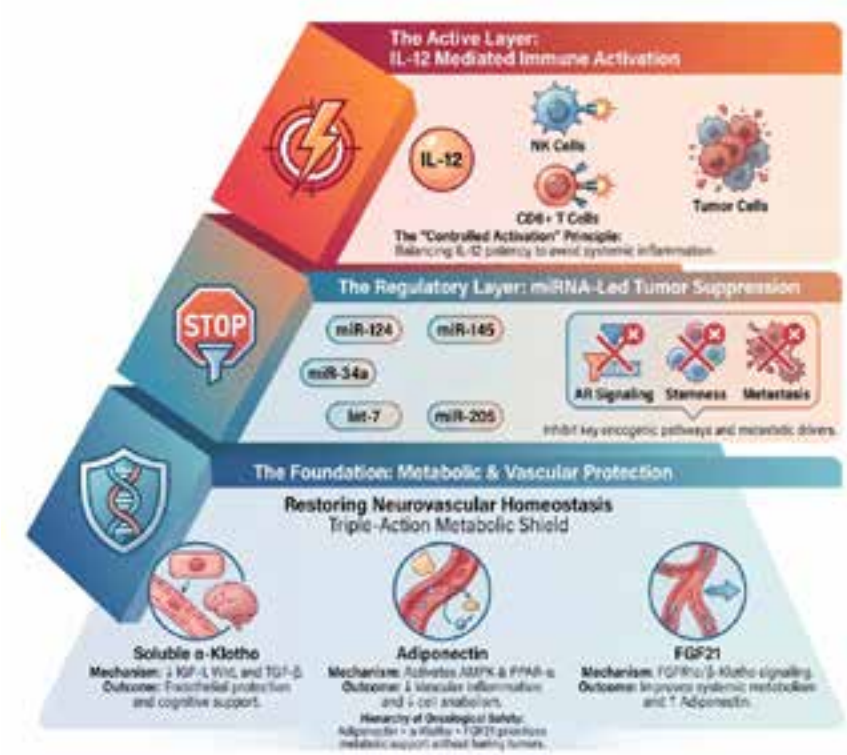

Figure 10: An integrated strategy for prostate cancer and vascular dementia, showing how growth-promoting components were removed and anti-oncogenic, vascular-stabilizing, metabolic, neuroprotective, and immune-activating components were prioritized after PSA elevation and prostate cancer diagnosis.

Another important aspect of this case is the avoidance of standard prostate cancer treatments that may adversely affect cognition or motivation in vulnerable patients [1,11]. Androgen deprivation therapy and radiotherapy are established options for prostate cancer, but previous reports have raised concerns regarding cognitive decline, dementia risk, fatigue, and reduced motivation in some older patients [1,11]. For a patient already affected by vascular dementia, preservation of daily function and quality of life is a central therapeutic goal. The present case therefore highlights the need for individualized cancer management in which tumor control, neurocognitive stability, vascular risk, and patient preference are considered together rather than in isolation.

Serial three-dimensional MRI and virtual endoscopic imaging also provided clinically useful information. In this patient, 3D prostate MRI enabled visualization of the relationship between the prostate, bladder, and adjacent organs and supported the absence of extracapsular extension or bladder invasion (Figure 8). Similarly, virtual carotid endoscopy allowed longitudinal assessment of intraluminal vascular abnormalities (Figure 5). These imaging approaches may help clinicians and patients understand disease status visually, especially when treatment is conservative or biologically targeted rather than immediately invasive.

This report has several limitations. It describes a single uncontrolled case, and the observed stabilization of PSA and imaging findings cannot be attributed causally to the anti-oncogenic cytokine and exosome cocktail. PSA normalization was not achieved, and long-term oncological outcomes remain uncertain. In addition, cognitive decline eventually progressed (Figure 1), particularly in verbal memory, indicating that the strategy did not completely prevent dementia progression. Nevertheless, this case proposes a practical framework for molecularly adjusting regenerative therapy when malignancy emerges: remove potentially growth-promoting factors, introduce anti-oncogenic signaling, monitor PSA and imaging closely, and continue evaluating cognitive and vascular status. Further studies are needed to determine whether this approach is safe, reproducible, and clinically meaningful.

CONCLUSION

This case suggests that cytokine- and exosome-based therapies may be adaptively modified when vascular dementia coexists with prostate cancer. Removal of growth factor–containing neuroregenerative components with theoretical tumor-promoting potential and introduction of an anti-oncogenic cytokine and exosome cocktail were followed by relative PSA stabilization and no radiological evidence of local invasion or bone metastasis, while cognitive decline remained limited during part of the follow-up period. Because this is a single uncontrolled case, efficacy and causality cannot be inferred, and further studies are required to evaluate safety, reproducibility, and clinical relevance.

ACKNOWLEDGEMENTS

The authors thank Ms. Sayuri Sato and Ms. Fernanda Diaz for the preparation of this manuscript.

AUTHOR CONTRIBUTIONS

Takuji Shirasawa contributed to clinical evaluation, data interpretation, manuscript drafting, and manuscript revision. Luis Carlos Aguilar Cobos contributed to the design of the cytokine- and exosome-based formulations, treatment concept, data interpretation, and manuscript revision. Both authors reviewed and approved the final manuscript.

ETHICAL APPROVAL OF STUDIES AND INFORMED CONSENT

Written informed consent was obtained from the patient for publication of this case report and accompanying clinical images.

DATA AVAILABILITY STATEMENT

The data supporting the findings of this case report are available from the corresponding author upon reasonable request, subject to protection of patient privacy and applicable ethical restrictions.

CONFLICT OF INTEREST

The authors declare no conflicts of interest.

REFERENCES

1. McHugh DJ, Root JC, Nelson CJ, Morris MJ. (2018). Androgen-deprivation therapy, dementia, and cognitive dysfunction in men with prostate cancer: How much smoke and how much fire? Cancer. 124(7):1326–1334.
2. Ilut S, Vesa SC, Vacaras V, Braita L, Dascalescu VC, Muresanu DF, et al. (2023). Biological Risk Factors Influencing Vascular Cognitive Impairments: A Review of the Evidence. Brain Sci. 13(7):1094.

3. Mok VCT, Cai Y, Markus HS. (2024). Vascular cognitive impairment and dementia: Mechanisms, treatment, and future directions. Int J Stroke. 19(8):838–856.
4. Shirasawa T, Cobos LCA. (2023). Cytokine-Induced Neurogenesis and Angiogenesis Reversed Cognitive Decline in a Vascular Dementia Patient with Hashimoto's Thyroiditis. ES J Case Rep. 4(1):1036.
5. Shirasawa T, Cobos LCA. (2026). Cytokine-Based Regenerative Treatment in Primary Sjögren Syndrome: A Case Report of the Improvement of Anti-SSA Antibodies, Salivary Gland Swelling, and Hippocampal Atrophy. Mathews J Case Rep. 11(3):1–16.
6. Shirasawa T, Cobos LCA. (2026). Alzheimer's Disease with Carotid Intraluminal Findings and Rheumatoid Arthritis–Like Symptoms: A Case Report. Mathews J Case Rep. 11(3):1–16.
7. Chen YF, Luh F, Ho YS, Yen Y. (2024). Exosomes: a review of biologic function, diagnostic and targeted therapy applications, and clinical trials. J Biomed Sci. 31(1):67.
8. Elemam NM, Hotait HY, Saleh MA, El-Huneidi W, Talaat IM. (2024). Insulin-like growth factor family and prostate cancer: new insights and emerging opportunities. Front Endocrinol (Lausanne). 15:1396192.
9. Liu G, Zhu M, Zhang M, Pan F. (2023). Emerging Role of IGF-1 in Prostate Cancer: A Promising Biomarker and Therapeutic Target. Cancers (Basel). 15(4):1287.
10. Benzo RM, Moreno PI, Fox RS, Silvera CA, Walsh EA, Penedo FJ, et al. (2023). Comorbidity burden and health-related quality of life in men with advanced prostate cancer. Support Care Cancer. 31(8):496.
11. Shim M, Bang WJ, Oh CY, Lee YS, Cho JS. (2022). Androgen deprivation therapy and risk of cognitive dysfunction in men with prostate cancer: is there a possible link? Prostate Int. 10(1):68–74.
12. Shirasawa T, Cobos LCA. (2024). Cytokine-induced Neurogenesis for the Prevention and Treatment of Alzheimer's Disease. Mathews J Case Rep. 9(9):1–12.
13. Shirasawa T, Cobos LCA. (2026). Cytokine-Induced Liver Regeneration for Alcoholic Cirrhosis Therapy. Mathews J Case Rep. 11(2):1–14.
14. Shirasawa T, Cobos LCA (2026). Cytokine-induced Neurogenesis for the Treatment of IVF-induced ASD. Mathews J Case Rep. 11(1):1-13..
15. Ahearn TU, Peisch S, Pettersson A, Ebot EM, Zhou CK, Graff RE, et al. Transdisciplinary Prostate Cancer P (2018) Expression of IGF/insulin receptor in prostate cancer tissue and progression to lethal disease. Carcinogenesis. 39(12):1431–1437.
16. Fairaq A, Shawky NM, Osman I, Pichavaram P, Segar L. (2017). AdipoRon, an adiponectin receptor agonist, attenuates PDGF-induced VSMC proliferation through inhibition of mTOR signaling independent of AMPK: Implications toward suppression of neointimal hyperplasia. Pharmacol Res. 119:289–302.
17. Hajare AD, Dagar N, Gaikwad AB. (2025). Klotho antiaging protein: molecular mechanisms and therapeutic potential in diseases. Mol Biomed. 6(1):19.
18. Lin Z, Pan X, Wu F, Ye D, Zhang Y, Wang Y, et al. (2015). Fibroblast growth factor 21 prevents atherosclerosis by suppression of hepatic sterol regulatory element-binding protein-2 and induction of adiponectin in mice. Circulation. 131(21):1861–1871.
19. Liu C, Kelnar K, Liu B, Chen X, Calhoun-Davis T, Li H, et al. (2011). The microRNA miR-34a inhibits prostate cancer stem cells and metastasis by directly repressing CD44. Nat Med. 17(2):211–215.
20. Liu C, Kelnar K, Vlassov AV, Brown D, Wang J, Tang DG, et al. (2012). Distinct microRNA expression profiles in prostate cancer stem/progenitor cells and tumor-suppressive functions of let-7. Cancer Res. 72:(13):3393–3404.
21. Stope MB, Erb HHH. (2026). The miR-143/145 cluster in prostate cancer: molecular regulation, context-dependent functions, and medical implications. Biology Direct 21(46).
22. Fu J, Imani S, Wu MY, Wu RC. (2023). MicroRNA-34 Family in Cancers: Role, Mechanism, and Therapeutic Potential. Cancers (Basel). 15(19):4723.
23. O'Neill CP, Dwyer RM. (2020). Nanoparticle-Based Delivery of Tumor Suppressor microRNA for Cancer Therapy. Cells. 9(2):521.

24. El Bezawy R, Tinelli S, Tortoreto M, Doldi V, Zuco V, Zaffaroni N, et al. (2019). miR-205 enhances radiation sensitivity of prostate cancer cells by impairing DNA damage repair through PKCepsilon and ZEB1 inhibition. J Exp Clin Cancer Res. 38(1):51.

25. Varambally S, Cao Q, Mani RS, Shankar S, Wang X, Ateeq B, et al. (2008). Genomic loss of microRNA-101 leads to overexpression of histone methyltransferase EZH2 in cancer. Science. 322(5908):1695-1699.

26. Morita S, Horii T, Kimura M, Ochiya T, Tajima S, Hatada I. (2013). miR-29 represses the activities of DNA methyltransferases and DNA demethylases. Int J Mol Sci. 14(7):14647–14658.

27. Shi XB, Ma AH, Xue L, Li M, Nguyen HG, Yang JC, et al. (2015). miR-124 and Androgen Receptor Signaling Inhibitors Repress Prostate Cancer Growth by Downregulating Androgen Receptor Splice Variants, EZH2, and Src. Cancer Res. 75(24):5309–5317.

28. Ponomarev ED, Veremeyko T, Barteneva N, Krichevsky AM, Weiner HL. (2011). MicroRNA-124 promotes microglia quiescence and suppresses EAE by deactivating macrophages via the C/EBP-alpha-PU.1 pathway. Nat Med. 17(1):64-70.

29. Glassman CR, Mathiharan YK, Jude KM, Su L, Panova O, Lupardus PJ, et al. (2021). Structural basis for IL-12 and IL-23 receptor sharing reveals a gateway for shaping actions on T versus NK cells. Cell. 184(4):983–999 e924.

30. Ullrich KA, Schulze LL, Paap EM, Muller TM, Neurath MF, Zundler S, et al. (2020). Immunology of IL-12: An update on functional activities and implications for disease. EXCLI J. 19:1563–1589.

31. DeBlaker-Hohe DF, Yamauchi A, Yu CR, Horvath-Arcidiacono JA, Bloom ET. (1995). IL-12 synergizes with IL-2 to induce lymphokine-activated cytotoxicity and perforin and granzyme gene expression in fresh human NK cells. Cell Immunol. 165(1):33-43.